Engineered Science
DOI: http://dx.doi.org/10.30919/es1807

Numerical Simulation of Conjugate Heat and Mass Transfer During Vacuum Freeze-drying of Mare Milk: Validation and Energy-optimisation Study

Ayaulym Rakhmatulina,[1, 2] Arshyn Altybay[3 ,4, 5,*] and Symbat Satybaldy[1, 6]

Abstract

Vacuum freeze-drying is a preferred method for converting mare's milk into a shelf-stable powder while retaining its nutritional and sensory qualities. However, the process remains time-consuming and energy-intensive. This study presents a validated three-dimensional numerical model that simulates conjugate heat- and mass-transfer during vacuum freeze-drying under industrially relevant conditions. The governing equations for heat conduction, water-vapour transport (Darcy's law), and latent-heat removal were solved in COMSOL Multiphysics 6.3 using the Deformed Geometry interface to track phase-front motion without remeshing. Simulations were performed on a 50 × 45 × 0.7 cm slab frozen to -50 ℃ with a shelf temperature of -20 ℃ and chamber pressure ranging from 15 to 35 Pa. Validation was conducted in a 0.45 m^2 pilot dryer using centre-line temperature measurements and gravimetric moisture-loss data. The model reproduced experimental temperature profiles (R^2 = 0.96) and predicted sublimation-front motion within 4% of image-based observations. Thinner samples (3 mm vs. 7 mm) and lower pressures (15 Pa vs. 35 Pa) significantly reduced drying time, though gains diminished below 15 Pa. This model offers a practical framework for optimising freeze-drying conditions and is extendable to other porous food and biopharmaceutical products.

Keywords: Conjugate heat and mass transfer; Numerical Simulation; Sublimation front; Vacuum freeze-drying; Mare milk powder; Energy optimization.

Received: 18 June 2025; Revised: 05 October 2025; Accepted: 08 October 2025.
Article type: Research article.

1. Introduction

Studies have shown that mare's milk is low in fat, easily digestible, and packed with essential vitamins and minerals. It also offers anti-ageing and restorative benefits, among other advantages.[1-5] In Kazakhstan, the production of mare's milk holds deep cultural significance and considerable economic potential. Unlike fresh mare's milk, which has a short shelf life, powdered mare's milk can be stored for extended periods without refrigeration, making it much easier to transport and store.

As global interest in health foods and natural products grows, mare's milk powder could carve out a niche in markets across Europe, North America, and Asia. Emphasising its distinctive nutritional profile and health benefits may attract a broader consumer base.

However, converting fresh mare's milk into powder is costly, necessitating specialised equipment and technology investment. One of the most effective methods for producing mare's milk powder is vacuum sublimation drying, which has shown promise in preserving the nutritional value and sensory qualities of the milk. Although freeze-vacuum drying is more energy-intensive and costly than other drying methods,

[1] *Department of Mechanical Engineering and Robotics, U. Joldasbekov Institute of Mechanics and Engineering, Almaty, 050000, Kazakhstan*
[2] *Department of Mechanical Engineering, Satbayev University, Almaty, 050000, Kazakhstan*
[3] *Department of Differential Equations, Institute of Mathematics and Mathematical Modeling, Almaty, 050010, Kazakhstan*
[4] *Department of Mathematics: Analysis, Logic and Discrete Mathematics, Ghent University, Ghent, 9000, Belgium*
[5] *Department of Computer Science, Al-Farabi Kazakh National University, Almaty, 050040, Kazakhstan*
[6] *Departments of Technological Machines and Equipment, Satbayev University, Almaty, 050000, Kazakhstan*
**Email:* arshyn.altybay@gmail.com (A. Altybay)

ongoing theoretical and experimental research aims to optimise this technology, reducing energy use and production costs.[3,4]

Numerous freeze-drying models have been proposed in various studiesto explain the process.[6-9] Of the various freeze-drying models in the literature, the sorption–sublimation model developed by Liapis and Litchfield is one of the most widely used.[8] This model incorporates both sorption and ice sublimation of moisture, but it is limited to a single spatial dimension, with the drying front moving forward as drying progresses.

Tang *et al*.[10] first introduced a two-dimensional framework for simulating the freeze-drying of pharmaceuticals in penicillin vials, enabling a more faithful depiction of the advancing sublimation front. Millman *et al.*[11] later generalised the approach to accommodate samples of virtually any geometry. Although this extended model is widely cited for its versatility and richer physics, its mathematical complexity and the large set of required parameters limit its routine industrial adoption.

In Scutella *et al.*[12] the impact of vial geometry on the heat transfer coefficient, and consequently on product quality, was investigated by predicting temperature distribution during the primary drying phase. The Uniformly Retreating Ice Front (URIF) model for freeze-drying was introduced by King,[13] which was later refined by Litchfield *et al.*[14] and Liapsis *et al*.,[15] forming the foundation of the sorption-sublimation model. A 2D axisymmetric finite element model for freeze-drying was developed by Mascarenhas *et al.*,[16] which calculates the transient changes in temperature, water vapour partial pressure, and the concentration of sorbed and bound water in the dried layer.

In Scutella *et al*.[17] presented a comprehensive three-dimensional (3D) mathematical model to simulate heat transfer during vial freeze-drying, emphasising the need to understand complex temperature gradients and heat fluxes that significantly affect drying efficiency and product quality. In a similar approach, Raja *et al.*[18] performed a numerical study on heat and mass transfer during the sublimation drying of milk in a vial, incorporating the effects of phase transitions and mass transfer behaviour. Their results highlight the importance of controlling heat transfer and moisture extraction, providing valuable guidance for improving freeze-drying efficiency in dairy applications.

Recent studies by El-Maghlany *et al.*[19] and Chen *et al.*[20] have substantially enhanced the understanding of freeze-drying, particularly regarding heat and mass transfer. In 2019, El-Maghlany *et al.*[19] introduced a multi-phase porous media transport model that accurately predicts temperature and moisture profiles during the drying process, supporting efforts to optimise freeze-drying efficiency. In 2023, Chen *et al.*[20] integrated computational simulations with experimental tests to study the vacuum freeze-drying of kiwifruit, offering useful knowledge for sectors handling sensitive materials. Freeze-drying enables precise structure preservation across fields: Khamitkyzy *et al*.[21] use antidiabetic cryoprotectants to maintain A. muciniphila viability, while Zhu *et al.*[22] employ vacuum freeze-drying to build robust CNT-silica aerogel monoliths - showing formulation and protocol control drives biological and materials performance. This study advances our prior research by incorporating 3D simulations,[23,24] vapour pressure evaluation, and a comprehensive parametric analysis. Through coupled numerical and experimental analysis, this work deciphers the governing heat and mass transfer phenomena in mare's milk sublimation drying. Resolving these mechanisms is pivotal for process optimisation, where predictive modelling reveals how thermal gradients, vapour diffusion, and material properties collectively dictate drying kinetics and final product attributes.

The paper is organised as follows: Section 2 describes the numerical simulation framework, covering the governing equations, initial and boundary conditions, parameters, thermophysical properties, and numerical methods. Section 3 presents the experimental measurements and compares the current predictions with other authors' findings and numerical results. In Section 4, we present and discuss our findings: we validate the numerical model against experimental data, examine the dynamics of the sublimation drying process, and provide comprehensive evaluations of heat and mass transfer. The paper concludes with a summary of the main findings and recommendations for future research.

2. Numerical simulation

Freeze-vacuum drying is highly effective in producing premium-quality products; however, it is characterised by substantial energy use and prolonged processing times, typically exceeding 25 hours. To mitigate these high experimental costs, numerical modelling has been employed to optimise process parameters and achieve more efficient drying conditions. The experimental arrangement involves trays measuring 50 cm by 45 cm with a depth of 3 cm, utilised for mare's milk drying at thicknesses ranging from 3 mm to 7 mm. Taking advantage of the symmetric properties of the experimental domain, we used a computational domain size of 1.5 cm x 1 cm x 0.7 cm to reduce the computation time of the simulation. The computational domain, as shown in Fig. 1, was divided into two separate zones: the dried top layer and the frozen bottom layer. Throughout sublimation, the interface between these two layers steadily advanced downward, progressively thickening the dried section. Completion of the

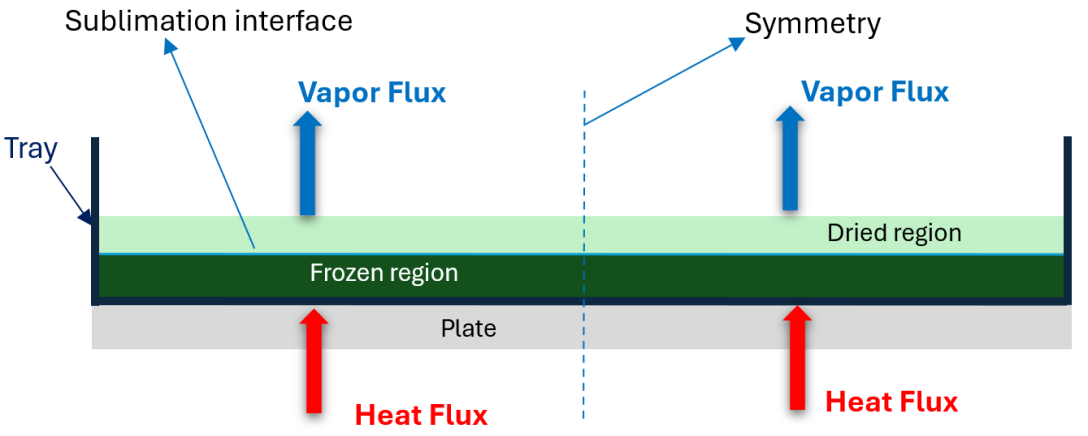

Fig. 1: Computational domain.

primary drying stage occurred once this sublimation front arrived at the bottom surface of the tray.

2.1 Assumptions

To facilitate the modelling approach adopted in this research, several simplifications have been introduced, inspired by the work of Lopez-Quiroga *et al.* [25] These include the following key considerations:

1. The structural integrity of the solid framework is assumed to remain unchanged throughout the process.
2. A distinct and negligible-thickness boundary is assumed to separate the frozen and dried zones.
3. Vapour movement within the dried portion is governed by the principles of Darcy's law.
4. The porous structure is assumed to retain its form, provided the temperature remains below the glass transition point.

2.2 Governing equations

The numerical model for vacuum freeze-drying of mare's milk couples heat and mass transport within a porous medium undergoing phase change. The system consists of two distinct regions: a frozen zone composed of ice and solid matrix, and a dry zone consisting of vapour and solid matrix. Sublimation at the interface leads to progressive growth of the dry layer and recession of the frozen layer.

2.2.1 Heat transfer

The temperature field $T(x,y,z,t)$ in the porous medium is governed by the energy conservation equation:[19]

$$(\rho c_p)_{eff}\frac{\partial T}{\partial t} + \rho_v c_{p,v}\vec{u}\cdot\nabla T = \nabla\cdot(k_{eff}\nabla T) + Q_{latent} \quad (1)$$

where $(\rho c_p)_{\text{eff}}$ is the effective volumetric heat capacity, k_{eff} is the effective thermal conductivity, $\vec{u}$ is the Darcy velocity of vapour, and Q_{latent} accounts for the latent heat absorption due to sublimation.

2.2.2 Vapor transport

Vapor mass transfer $\vec{u}$ (m/s) is derived from Darcy's law, expressed as:[19]

$$\vec{u} = -\frac{K_d}{\mu_v}\nabla p_v \quad (2)$$

where K_d is the permeability of the dried porous medium, μ_v is the dynamic viscosity of the water vapour, and p_v is the vapor pressure. The relationship between vapour pressure and vapour density is maintained via the ideal gas approximation.

The corresponding water vapour pressure p_v is calculated from the vapour density ρ_v using the ideal gas law:[19]

$$p_v = \frac{\rho_v RT}{M_v} \quad (3)$$

where R denotes the universal gas constant, and M_v represents the molecular mass of water vapour.

2.2.3 Sublimation interface and phase change

The sublimation interface is tracked using a moving boundary approach based on the Clausius-Clapeyron relation:[19]

$$T_s = \frac{\Delta H_s M_v}{R\ln\left(\frac{p_0}{p_v}\right)} \quad (4)$$

where T_s is the sublimation temperature, ΔH_s is the latent heat of sublimation, p_0 is a reference pressure, and p_v is the vapor pressure at the interface.

The movement of the sublimation front is governed by mass conservation:[19]

$$\rho_i\frac{dH}{dt} = -\rho_v\vec{u}\cdot\vec{n} \quad (5)$$

where $H(t)$ is the interface position and $\vec{n}$ is the normal vector

pointing outward from the frozen domain. This equation ensures that the vapour flux at the interface corresponds to the rate of ice removal due to sublimation.

Eqs. (1)-(5) adopt the porous-medium framework validated in our previous two-dimensional study;[21] however, all thermo-physical properties have been re-estimated for the present three-dimensional geometry using the experimental data.

2.3 Initial and boundary conditions

In this subsection, we set the initial Eq. (6) and boundary conditions Eqs. (7)-(13) for the governing equations. At the start of the sublimation phase (t = 0), we assume:

1. The pressure throughout the dried region equals the drying chamber pressure

2. The sample—comprising both frozen and dried layers—is isothermal at a uniform temperature

Accordingly, the initial conditions can be written as

$$T|_{t=0} = T_0, p|_{t=0} = p_c \quad (6)$$

wherer p_c refers to the pressure inside the drying chamber (measured in Pascals), and T_0 indicates the initial temperature of the sample material (in Kelvin) at the onset of the sublimation drying stage.

The mass-transfer boundary conditions at the top surface can be written in pressure—flux form as:

$$p|_{z=l_z} = p_c \quad (7)$$

At the lateral surface:

$$p|_{\omega_x} = p_c \quad (8)$$

As water vapour is generated at the moving sublimation front $x = H(t)$, mass conservation at this interface yields the following vapour-flux boundary condition:

$$-\rho_v \frac{k_m}{\mu_v} \nabla p|_{H(t)} = \frac{\partial H(t)}{\partial t}(\rho_f - \rho_d) \quad (9)$$

Here, $H(t)$ denotes the location of the sublimation front at time t. In this study, the sublimation process progresses in both the x- and y-directions. The heat transfer boundary conditions:

Bottom boundary: convective heat flux from the shelf:

$$-k_{\text{eff}} \nabla T \cdot \vec{n} = h(T_s - T) \quad (10)$$

where h is the heat transfer coefficient, and T_s is the shelf temperature.

Top and lateral boundaries: convective and radiative heat losses:

$$-k_{\text{eff}} \nabla T \cdot \vec{n} = h_{amb}(T - T_{amb}) + \sigma\epsilon(T^4 - T_{amb}^4) \quad (11)$$

In this context, h_{amb} represents the ambient heat transfer coefficient, σ is the Stefan–Boltzmann constant, and ϵ denotes the surface emissivity.

The heat transfer boundary conditions at the sublimation interface:

$$T_d|_{H(t)} = T_f|_{H(t)} = T_{sub} \quad (12)$$

$$k_f \nabla T_f|_{H(t)} - k_d \nabla T_d|_{H(t)} = T_f|_{H(t)} = \frac{\partial H(t)}{\partial t}(\rho_f - \rho_d)\Delta H_s \quad (13)$$

where T_{sub} refers to the temperature at the sublimation interface, measured in Kelvin.

2.4 Key parameters and thermal-physical characteristics of the materials

Because reliable experimental measurements of mare's milk's thermal conductivity, density, and specific heat capacity are unavailable, these thermophysical properties were approximated using its known compositional data. Table 1 summarises the standard compositional breakdown of mare's milk.[26]

Table 1: Composition of mare's milk.[26]

Component	Mass fraction (%)
Water	89.86
Lactose	6.37
Protein	2.14
Fat	1.21
Minerals (Ash)	0.42

Based on the given composition of mare's milk, the following solid matrix properties were estimated: km = 0.2757 W/m·K (thermal conductivity), ρ_m=1393.3 kg/m³ (density), $c_{p,m}$=1610.7 J/kg·K (specific heat capacity).

To capture the spatial variation of thermophysical properties during the sublimation process, volume-averaged properties were introduced. These depend on the local ice saturation level, denoted by S, which varies from 1 (fully frozen region) to 0 (completely dried region), with intermediate values representing the transitional sublimation zone.

The volume-averaged effective density and heat capacity were defined as:

$$(\rho c_p)_{\text{eff}} = (1-\varepsilon)\rho_m c_{p,m} + \varepsilon\rho_I c_{p,I} + \varepsilon(1-S)\rho_v c_{p,v} \quad (14)$$

Similarly, under the parallel conduction model for porous media, the effective thermal conductivity was given by:

$$k_{\text{eff}} = (1-\varepsilon)k_m + \varepsilon S k_I + \varepsilon(1-S)k_v \quad (15)$$

Table 2: Simulation parameters for the freeze-drying procedure.

Parameter	Value	Units	Source
ε	0.705	-	[27]
ρ_m	1399.3	kg/m ^{3}	
$c_{p,m}$	1610.7	$k \cdot J/kg \cdot K$	
k_m	0.2757	W/m · K	
ρ_I	913	kg/m ^{3}	[28]
$c_{p,I}$	2.090	kJ/kg · K	[28]
k_I	2.22	W/m · K	[28]
ρ_v	$\frac{pM_v}{RT_{dry}}$	kg/m ^{3}	[20]
$c_{p,v}$	1.866	kJ/kg · K	[28]
k_v	0.0022	W/m · K	[28]
μ_v	$0.11(T/273)^{1.5}/(T+961)$	kg/m · s	[28]
M_v	0.018	kg/mol	[19]
R	8.314	J/mol · K	[19]
K_d	$(1-S)\times 10^{-18}(1+6.68\times 10^5/p)$	m ^{2}	[28]
ΔH_{sub}	2821	kJ/kg	[28]

In Eq. (14), ρ and c_p denote density and specific heat, respectively, and in Eq. (15) k denotes thermal conductivity; subscripts m, I, v refer to solid matrix, ice, and vapour, and ε is porosity.

By setting $S = 0$, one obtains the thermophysical properties corresponding to the fully dried state of the product, as reported by El-Maghlany *et al.*[19]. An overview of the parameters used in the numerical simulation is provided in Table 2.

2.4.1 Numerical method

The numerical simulation was conducted using a three-dimensional model implemented in COMSOL Multiphysics 6.3, leveraging the finite element method (FEM) to solve coupled heat and mass transfer equations during vacuum freeze-drying in a porous medium. The governing equations were addressed through the Heat Transfer in Porous Media and Darcy's Law modules, capturing thermal conduction and vapour transport, respectively, within the porous frozen milk domain.

The domain was initially assumed to be fully frozen, with phase change tracked by a Phase Change Interface feature, which used a temperature-dependent condition to identify the sublimation front. A Deformed Geometry module was incorporated to handle mesh deformation associated with volume reduction during ice sublimation.

The bottom surface was subjected to a prescribed heat flux (representing heating from the shelf), while lateral and upper boundaries were thermally insulated. Time-dependent studies were performed over a simulation window of up to 24 hours using a Backward Differentiation Formula (BDF) time-stepping scheme. To enhance solver robustness, a segregated approach was adopted with two segregated steps: one for the pressure field and one for the temperature field, each solved using PARDISO, a direct linear solver. For nonlinear acceleration, Anderson acceleration was enabled with a damping factor of 0.9, and Jacobian updates were performed once per time step.

Stop conditions were defined using custom expressions to terminate the simulation once the sublimation front approached the bottom of the domain. The thermal and physical properties were assigned using a homogenised porous media approach, including the newly calculated values for dry mare's milk and ice.

2.4.2 Mesh-independence study

A swept hexahedral mesh was generated by first discretising the lower surface with *Free-Triangular* elements and then extruding the pattern along the z-axis. Four inflation layers (r = 1.2) were applied at the sublimation front and shelf interfaces to resolve steep temperature gradients. Three global resolutions were tested -4.8 × 10^5, 8.2 × 10^5 and 1.4 × 10^6 cells-while keeping the local boundary refinement at the *Extra-fine* level. The maximum difference in product-centred temperature between the two finest grids did not exceed 1.7 K and the predicted drying time varied by less than 1.9 %. Consequently, the intermediate mesh 8.2 × 10^5 cells, minimum quality 0.34) was adopted for all simulations. During

deformation, node movement was stabilised with *hyperelastic smoothing*, eliminating the need for remeshing and maintaining mesh skewness below 0.35 throughout the drying period.

The 3D conjugate heat-and-mass transfer model described above yields detailed predictions of centre-line temperature histories, moisture-loss curves, and sublimation-front trajectories for each sample thickness and chamber pressure. In the following Section 3, we present the experimental apparatus, measurement protocols, and data-processing methods used to obtain triplicate measurements of temperature, mass loss, and interface position, against which these numerical outputs are directly validated.

3. Experimental setup and data acquisition

Building on the previously presented vacuum freeze-drying model, this section details an experimental study of mare's milk under vacuum freeze-drying conditions, designed to validate the numerical simulation results.

3.1 Experimental apparatus

The experiments were carried out using a shelf-type vacuum freeze-dryer (model ZLGJ-300) manufactured by Zhengzhou Huachen (China), as illustrated in Fig. 2. Detailed specifications can be found in the work of Rakhmatulina *et.al*.[23]

The sample was loaded into the drying chamber, where, under low temperature and reduced pressure, the ice phase sublimated directly into vapour. This vapour was then drawn through a vacuum line into the condenser, where it was re-deposited as either solid or liquid.

3.2 Experimental procedure

In this study, the samples were poured into stainless steel trays measuring 50 × 45 × 3 cm. To examine the impact of layer thickness on the drying process, mare's milk was distributed to varying heights of 0.3, 0.5, and 0.7 cm. The trays were subsequently placed inside the vacuum freeze-drying chamber for experimentation.

Before initiating the sublimation process, a temperature sensor was embedded in the sample to monitor changes in internal temperature. To ensure complete solidification of the milk, the samples were pre-frozen at -50 °C for 2-3 hours. Once frozen, the chamber pressure was gradually reduced from atmospheric pressure (10^5 Pa) to a vacuum level of 15 Pa. Simultaneously, heat was supplied via the shelves to initiate sublimation. Sublimation drying, recognised as the most energy-demanding stage of vacuum drying, was carried out under consistent low-pressure and low-temperature conditions. The weight of each sample was recorded every three hours to monitor moisture loss, with moisture content calculated from the reduction in mass. In addition, the system automatically logged temperature and pressure data at three-minute intervals throughout the drying period. The entire sublimation process lasted between 22 and 25 hours, depending on the thickness of the milk layer.[23] Drying was considered complete once the sample weight stabilised, signifying that all the free moisture had been successfully removed. An image of the dried product is presented in Fig. S1.

The moisture content of mare's milk during vacuum sublimation drying was tracked using an Evlas-2M moisture analyser, a high-precision device specifically designed for moisture determination in food and biological samples. Dried samples were collected every 3 hours, cooled to room temperature, and weighed before and after drying using a high-precision balance. Moisture content was calculated as in Eq. (16):

$$\text{Moisturecontent}(\%) = \frac{W_2 - W_3}{W_2 - W_1} \times 100 \qquad (16)$$

where W_1 is the weight of the empty container, W_2 is the weight of the container with the sample before drying and W_3 is the weight of the container with the sample after drying. Measurements were averaged over three trials, confirming a final moisture content below 4%, in line with industry standards. The analyser was regularly calibrated, and the results were used to validate the numerical model.

All freeze-drying experiments were performed in triplicate (n = 3) for each sample thickness (3, 5, and 7 mm) and chamber pressure (15, 25, and 35 Pa). Variability is reported as standard deviations: for centre-line temperature SD ≤ 1.5 °C (95 % CI) with a maximum trial-to-trial drying-time variation of 4 %; for gravimetric measurements (moisture content and mass loss) SD ± 0.3 % and ± 0.02 g, respectively.

4. Results and discussion

4.1 Experiment and simulation verification

Several experiments were carried out using sample thicknesses of 3, 5, and 7 mm, under chamber pressures of 15, 25, and 35 Pa. Initially, the sample was placed in the chamber. A temperature sensor was then inserted into the sample to track internal temperature variations. To achieve full solidification of the milk, the samples were pre-frozen at - 50 °C for 2-3 hours. After freezing, the chamber pressure was gradually lowered from atmospheric pressure (10^5 Pa) to a vacuum level of 15 Pa. During the sublimation stage, the temperature was increased stepwise until reaching the target value. These stepwise changes were incorporated into the numerical simulation.[23]

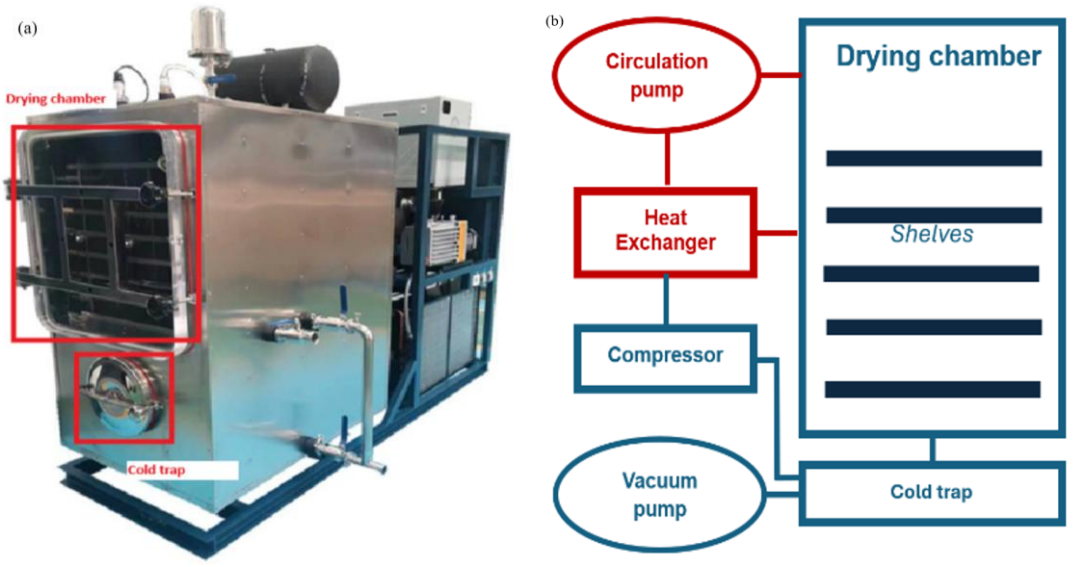

Fig. 2: The apparatus (a) and design layout of the shelf-type vacuum freeze-drying unit (b).

Fig. 3 presents a direct comparison of simulated and experimental temperature curves during both the primary and secondary drying phases for the 7 mm thick sample. Measurements were recorded at the tray's centre, where the mare's milk was situated.

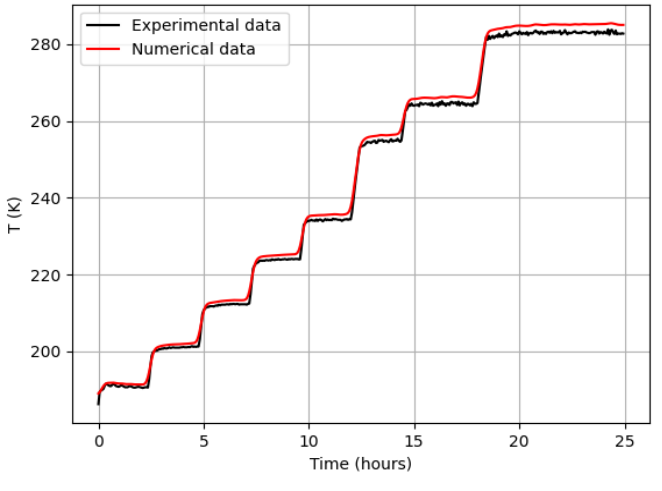

Fig. 3: Comparison between the measured and simulated temperatures (sample thickness of 7 mm).

Fig. 3 demonstrates a strong correlation between the numerical simulation results and the experimental temperature data. In the simulation, both cooling and heating from beneath the tray were implemented using a stepwise function.

During the initial stage of sublimation drying, significant latent heat is absorbed for ice sublimation, causing a drop in the sample temperature. As the sublimation front advances, the temperature of the dried layer surface rises, while the frozen zone temperature stays slightly lower than the shelf temperature. During the last ten hours of drying, there is a significant discrepancy between the experimental and modelled data. The simulated temperature rapidly attains the shelf temperature, while the experimental temperature exhibits a slower increase. This discrepancy indicates that the model overestimates the heat transfer efficiency from the shelf compared to the actual experimental conditions. A likely reason for this is the constant pressure in the chamber.

To evaluate the model's predictive performance, the coefficient of determination (R^2) was calculated using the following Eq. (17):

$$R^2 = 1 - \frac{\sum (y_i - \hat{y}_i)^2}{\sum (y_i - \bar{y})^2} \quad (17)$$

where y_i are the experimental temperature measurements, $\hat{y}_i$ are the simulated values, and $\bar{y}$ is the average of the experimental data. The high R^2 value of 0.96 demonstrates a strong correlation between the simulated and experimental results throughout both sublimation and drying phases, confirming the model's accuracy in predicting thermal behaviour. As illustrated in Fig. 3, the model accurately reproduces the temperature evolution, confirming its reliability in capturing the heat and mass transfer dynamics of the sublimation drying process.

To validate the simulation results, the model was benchmarked against published data from for skim milk freeze-drying.[25] As illustrated in Fig. 4, both the predicted temperature profiles and sublimation front progression show strong consistency with these reference findings.

The same 3D conjugate transport model was validated for all sample thicknesses (3, 5, 7 mm) and chamber pressures (15-35Pa) Validation for 3 mm and 5 mm samples showed comparable accuracy (R^2 = 0.94-0.97) to the 7 mm case (Fig.

4), confirming model robustness across geometries.

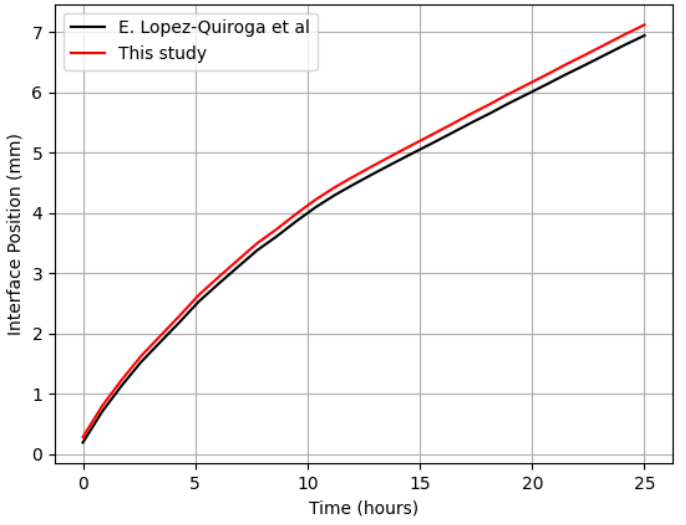

Fig. 4: Comparison between the predicted sublimation front progression in this study and published reference data.[25]

4.2 Sublimation drying process analysis

To analyse heat and mass transfer in mare's milk during freeze-drying, a specific set of parameters was selected as the baseline for simulation. These conditions included a sample thickness of 7 mm, a shelf temperature of -20 °C, and a chamber pressure of 35 Pa.

Fig. 5 illustrates the progression of the sublimation front under these standard conditions. The frozen portion of the sample (represented in grey) gradually shrinks over time, receding toward the base of the sample as the dried layer expands. Because water vapour can only escape through the top surface, the sublimation front advances unidirectionally along the vertical (z) axis.

During the initial phase of drying, sublimated vapour is rapidly expelled from the upper surface, leading to a quick expansion of the dried zone. However, as the process continues, the increasing distance between the sublimation front and the surface causes slower vapour diffusion, reducing

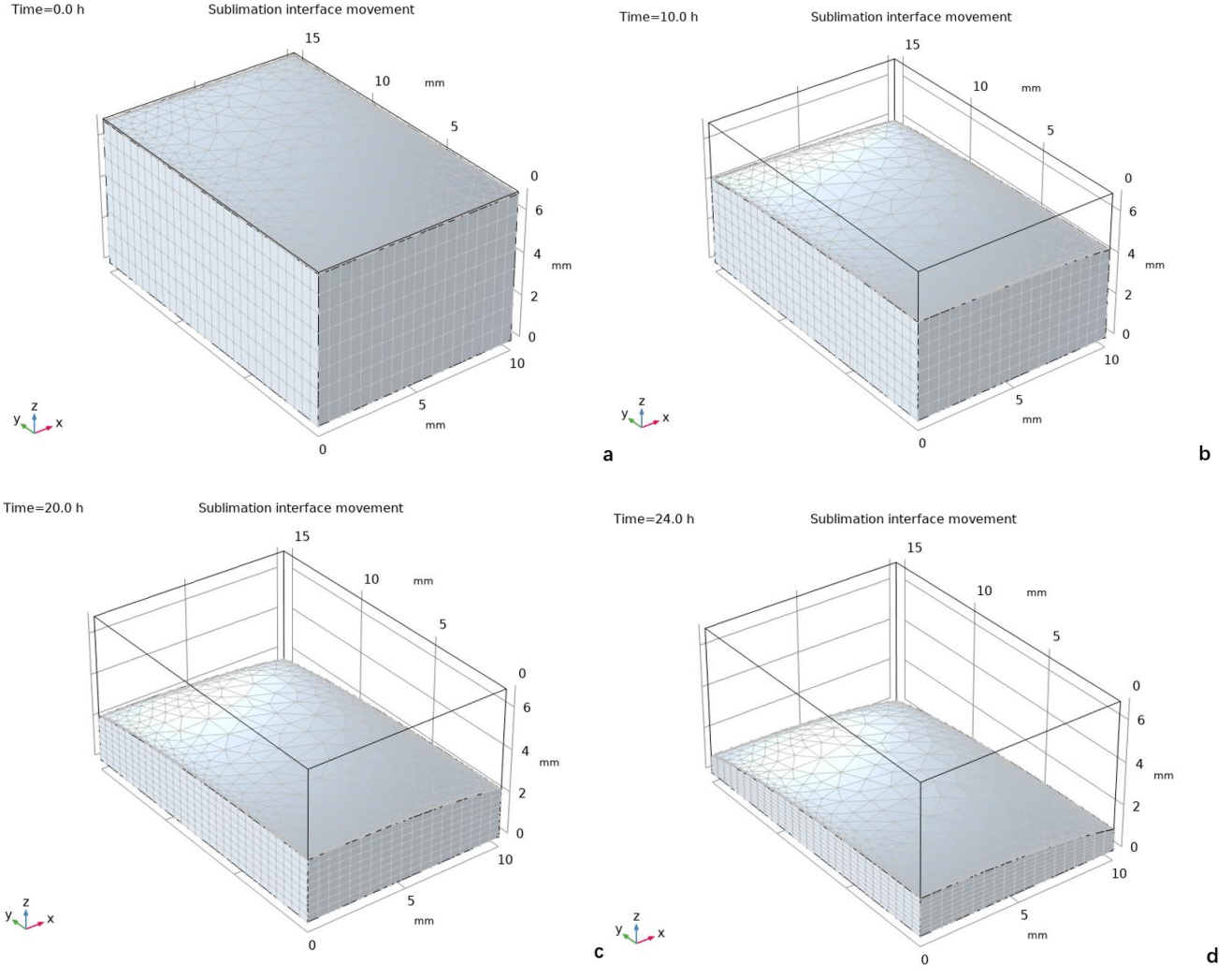

Fig. 5: Progression of the sublimation interface during the drying process at the following time points: (a) 0 hours, (b) 10 hours, (c) 20 hours, and (d) 24 hours.

the rate at which the interface moves. By the final stage, the remaining ice crystals near the sample's bottom become highly resistant to sublimation, demanding significant energy input for complete removal.

4.3 Heat transfer analysis

The study examined temperature variations and heat flow within the drying chamber, with simulations highlighting strong thermal gradients in the initial drying phase. These gradients arise from the substantial energy demand of the ice-to-vapour phase transition.

Under standard freeze-drying conditions, Fig. 6 displays the evolving temperature profile of mare's milk samples. Heat from the shelf propagates through the frozen layer toward the sublimation front, driving the drying process.

A critical distinction exists between the frozen and dried zones in terms of thermal properties. The frozen portion, with its greater thermal conductivity and heat capacity, maintains steadier temperatures and warms more gradually. In contrast, the porous dried layer absorbs radiative heat more efficiently, causing faster localised heating.

4.4 Mass transfer analysis

Fig. 7 presents the vapour pressure distribution observed in mare's milk samples under standard freeze-drying conditions. The computational model, which excludes mass transfer considerations in the frozen zone, focuses exclusively on pressure variations within the dried region.

4.5 Sensitivity analysis

To assess the robustness of the numerical model and quantify the influence of key input parameters on drying performance, a global sensitivity analysis was conducted using the Morris elementary effects method Eq. (18). Three critical parameters - Darcy permeability (K_d), effective thermal conductivity (k_{eff}), and latent heat of sublimation (ΔH_{sub}) were perturbed by $\pm 10\%$ from their baseline values (Table 3). Simulations were performed under standard conditions (7 mm thickness,

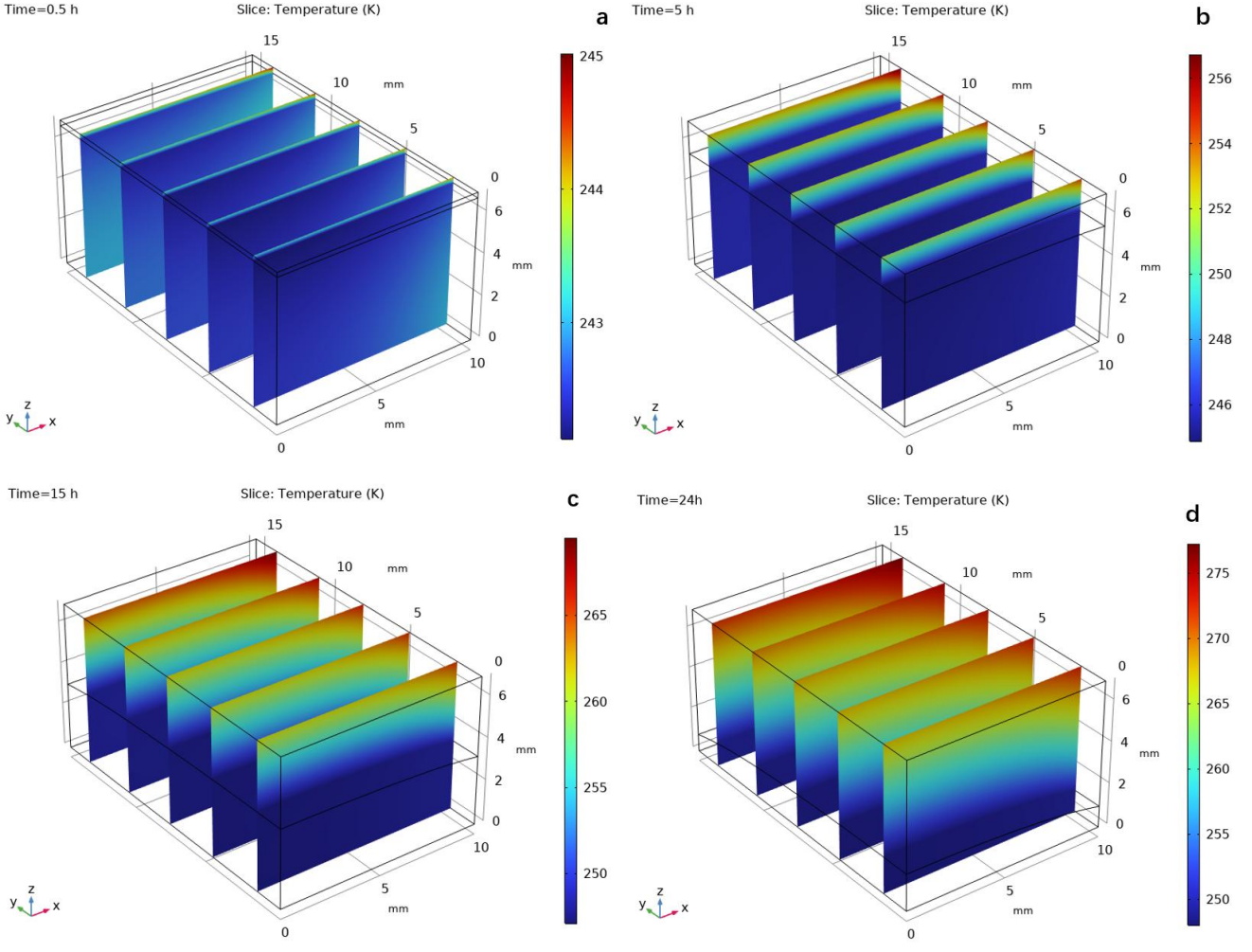

Fig. 6: Heat flux distribution (K) at different stages of the drying process.

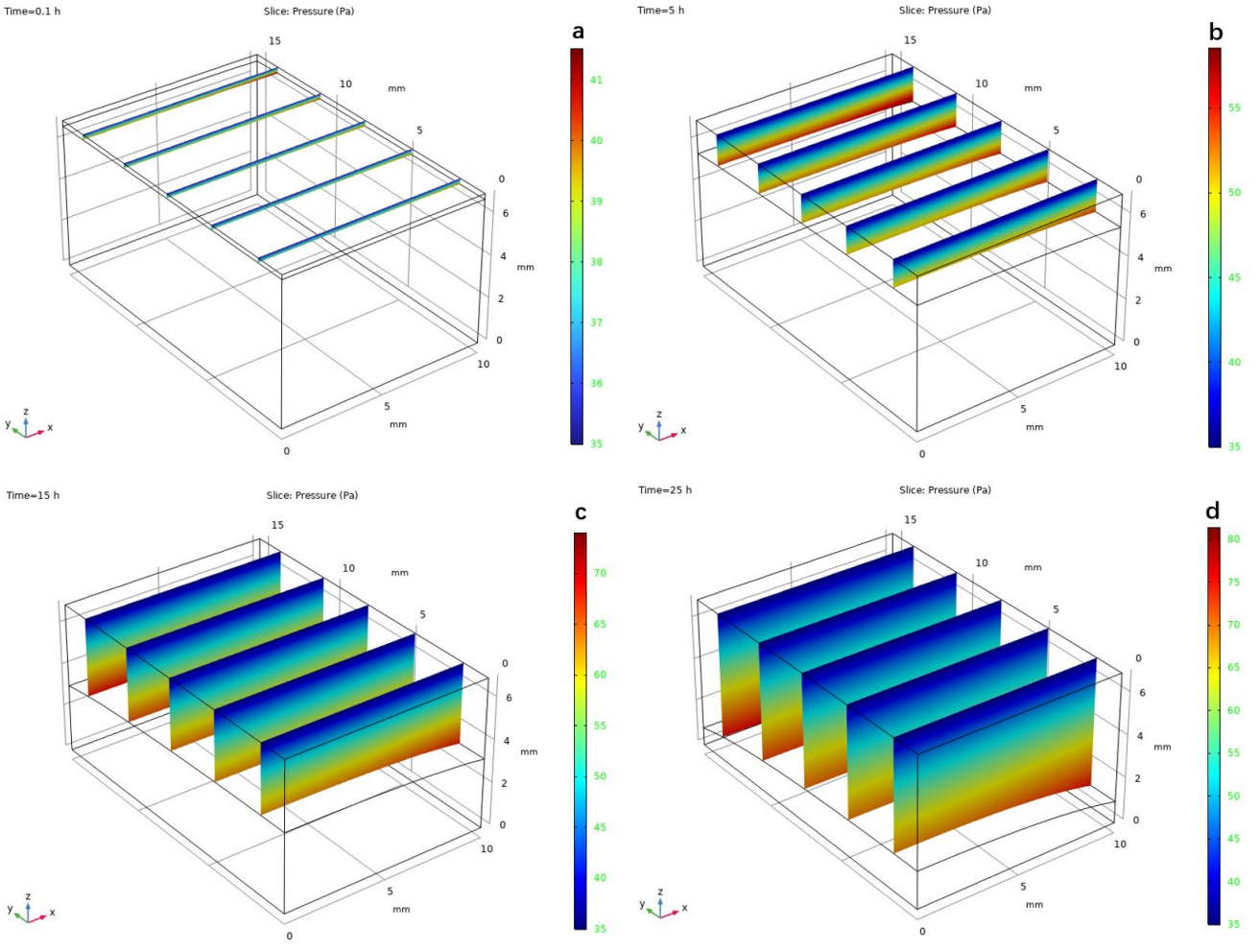

Fig. 7: Vapour pressure distribution (Pa) throughout the sublimation drying process at different time intervals: (a) 0.1 hours, (b) 5 hours, (c) 15 hours, and (d) 25 hours.

35 Pa pressure, -20 °C shelf temperature), with drying time (to 4% moisture content) as the output metric.

The elementary effect EE_i for parameter i was computed as:

$$EE_i = \frac{f(x_1,\ldots,x_i+\Delta,\ldots,x_k)-f(\mathbf{x})}{\Delta} \quad (18)$$

where $f(\mathrm{x})$ is the drying time at baseline, $\Delta = 0.1$ (10 % perturbation), and $k = 3$ parameters. Normalised sensitivity coefficients (S_i) were calculated as:

$$S_i = \frac{EE_i}{\max(EE_i)} \times 100\% \quad (19)$$

The results of the sensitivity analysis for the key parameters are presented in Table 3.

As a result of the sensitivity analysis Eq. (19), we observed the following key findings:

• Permeability (K_d) dominates sensitivity, contributing 68 % to drying-time variability. A 10 % decrease in K_d prolongs the drying time by 11.5 %, as reduced vapour transport efficiency

Table 3: Sensitivity analysis results for key parameters.

Parameter	Baseline value	Perturbation	Drying time (h)	Δ Time (%)	S_i (%)
K_d (Permeability)	$(1-S)\times 10^{-18}(1+6.68\times 10^5/p)$ m ^{2}	+10%	19.1	−4.5	68
		−10%	22.3	+11.5	
k_{eff} (Thermal cond.)	Eq. (15)	+10%	20.8	+3.9	22
		−10%	19.2	−4.2	
ΔH_{sub} (Latent heat)	2821 kJ/kg	+10%	21.7	+8.6	10
		−10%	18.6	−6.9	

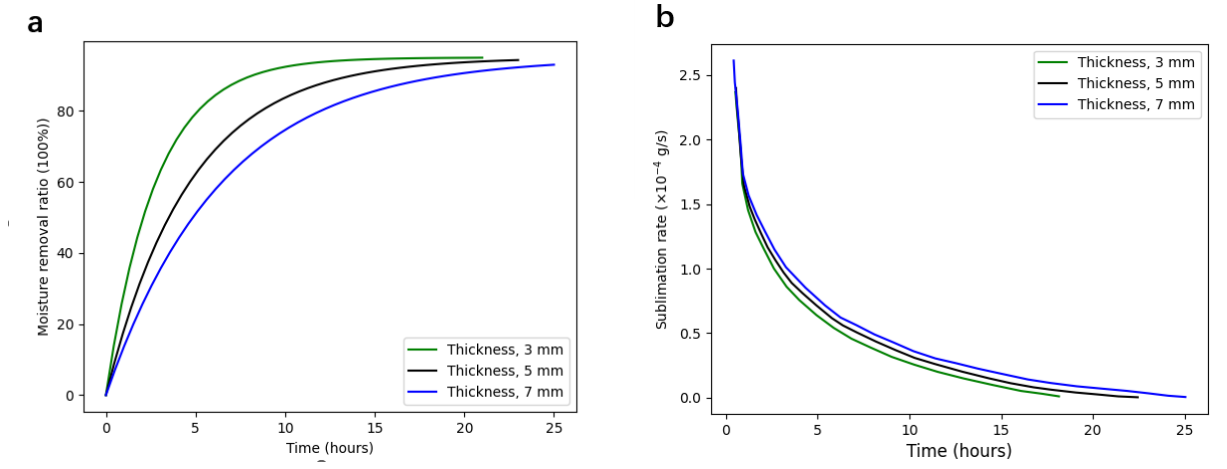

Fig. 8: Influence of sample thickness on (a) moisture removal efficiency and (b) sublimation kinetics during vacuum freeze-drying.

slows sublimation.

• Thermal conductivity (k_{eff}) accounts for 22 % of sensitivity. While higher conductivity accelerates heat delivery to the sublimation front, its impact is limited by the inherently slower vapour diffusion process.

• Latent heat (ΔH_{sub}) has minimal impact (10 %), since the heat supplied by the shelf largely buffers variations in sublimation enthalpy.

Together, these results confirm that vapour transport limitations - rather than thermal resistance or latent-heat effects-control the primary-drying kinetics of mare's milk. Consequently, future experimental work should focus on accurately measuring and modelling permeability to improve the predictive power of the freeze-drying model.

4.6 Parametric study

In this subsection, a detailed parametric analysis is conducted, focusing specifically on critical variables such as sample thickness and chamber pressure, to understand their impact on the heat and mass transfer during the sublimation drying of mare's milk. The effect of sample thickness on moisture removal efficiency was investigated by varying thicknesses between 3 mm and 7 mm, while maintaining a constant shelf temperature of -20 °C and a chamber pressure of 35 Pa.

Fig. 8(a) demonstrates the impact of varying sample thicknesses on moisture removal. This graph displays the moisture removal ratio as a function of drying time for samples with thicknesses of 3 mm, 5 mm, and 7 mm. It is evident that thinner samples exhibit a more rapid moisture removal rate. Specifically, the 3 mm sample, indicated by the green line, achieves approximately 95% moisture removal within about 10 hours. Conversely, the 5 mm sample, marked by the black line, takes roughly 15 hours to attain the same moisture level. The 7 mm sample, shown with a blue line, displays the slowest drying progression, reaching 90% moisture removal after nearly 20 hours. This result highlights that thinner samples dry faster due to shorter moisture diffusion paths, which enable quicker moisture evaporation. Recognising this trend is essential for optimising vacuum sublimation drying processes, as sample thickness significantly influences drying efficiency and duration. Fig. 8(b) depicts the impact of sample thickness on the sublimation rate. The results indicate that increasing sample thickness enhances the sublimation rate, suggesting that thicker samples can release a greater amount of water vapour within a specific timeframe.

Fig. 9 illustrates the influence of chamber pressure on moisture removal efficiency and sublimation rate. The analysis includes three distinct chamber pressures: 15, 25 and 35 Pa. From Fig. 9(a), it is evident that reducing chamber pressure by every 10 Pa shortens drying time by approximately 0.5 hours; however, this also results in higher overall energy usage by the vacuum system. According to Fig. 9(b), a reduction in chamber pressure slightly boosts the sublimation rate during the initial drying phase. Nevertheless, beyond the 5-hour mark, sublimation rates stabilise across all pressures, indicating that the impact of chamber pressure is more pronounced initially and becomes less significant over time. However, as drying progresses and the dried region thickens, the vapour pressure at the sublimation interface stabilises, diminishing the effect of chamber pressure variations. The results indicate that although lowering the chamber pressure improves drying efficiency, its influence is relatively limited compared to factors like shelf temperature and sample thickness. The experimental results demonstrate that maintaining sample thickness below 7 mm ensures compliance with international quality standards ($< 4\%$ residual moisture) during vacuum freeze-drying. Samples

with greater thickness tend to retain more residual moisture, which can negatively affect the final product's quality and reduce its shelf life. Additionally, adjusting chamber pressure plays a crucial role in optimising drying efficiency. Lower chamber pressures typically enhance moisture removal ratios and initially increase sublimation rates, especially during the early drying stages. However, the influence of chamber pressure becomes less significant as the drying process progresses. Therefore, careful management of both sample thickness and chamber pressure is essential to achieve optimal drying outcomes and maintain product quality.

In industrial operations, scaling up freeze-drying processes by utilising larger trays to manage substantial sample quantities and installing multiple trays in the chamber can significantly enhance cost-effectiveness. This strategy boosts production rates without sacrificing product integrity, making it ideal for high-volume demands. Conversely, processing thin samples in smaller trays often proves inefficient, as it leads to higher energy expenditures and extended drying cycles relative to the output generated-factors that diminish economic viability.

Industrial Implications. Each 3D simulation of a 7 mm slab at a single pressure level requires approximately 2 hours of wall-clock time on an 8-core Intel Xeon (2.4 GHz) workstation with 32 GB Random Access Memory (RAM), using a mesh of 200k elements. For larger, factory-scale geometries (*e.g.* 1 m^2 trays), mesh coarsening strategies and parallel execution on a high-performance cluster (16–32 cores) reduce runtimes to under 24 hours per case. This demonstrates that, with standard High Performance Computing(HPC) resources and straightforward mesh optimisation, our model can be feasibly applied to production-scale freeze-drying design and optimisation.[29]

Looking ahead, upcoming research will concentrate on refining the freeze-drying technique through predictive modelling algorithms and automated monitoring systems. These innovations seek to harmonise product excellence with cost efficiency, addressing challenges in energy use and operational timelines. By focusing on adaptable frameworks, such advancements aim to facilitate the commercial scalability of vacuum sublimation drying, particularly for specialised applications like preserving mare's milk. This dual emphasis on quality and practicality could pave the way for sustainable large-scale adoption in diverse industries.

We note the following limitations of our current model. It assumes a constant porosity and undeforming solid framework, which may not hold for materials exhibiting significant shrinkage or collapse; it neglects frozen-zone mass transfer and does not capture secondary drying dynamics; and its mesh and solver settings are optimized for small slabs ($\leq 7mm$), so very large or geometrically complex samples may require further mesh refinement and parameter recalibration.

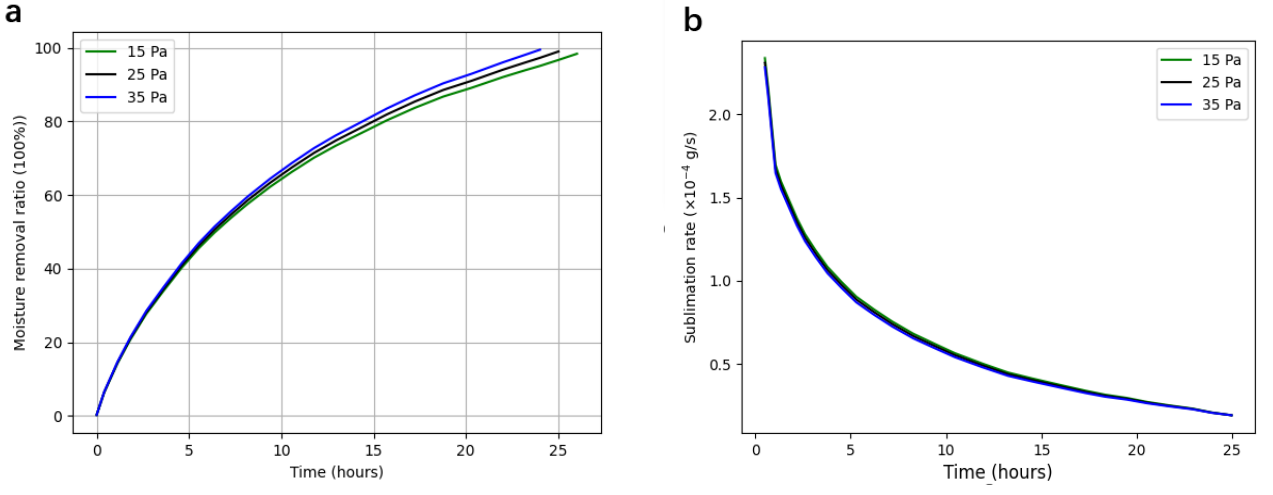

Fig. 9: Effect of chamber pressure on the (a) moisture removal ratio, (b) sublimation rate.

Table 4: Drying time, energy consumption, and SEC at 35 Pa.

Thickness	Time	Energy	SEC
3	9	130.5	134.3
5	14	203.0	209.0
7	25	362.5	373.1

4.7 Energy performance analysis

Assessing energy efficiency is crucial for sustainably scaling freeze-drying operations. Specific energy consumption (SEC) was calculated as the ratio of total energy input to water removed. Using our model $ZLGJ-300$ freeze dryer (rated power $14.5kW$) and a fixed water removal of 0.97 kg per batch, the total energy for each thickness at 35 Pa is $E_{total} = 14.5\ kW \times t$, and $SEC = \frac{E_{total}}{0.97\ kg}$. For samples of different thickness at 35 Pa, the drying time, energy consumption and SEC are given in Table 4. SEC increases with sample thickness: thinner layers dry faster, reducing energy per kilogram of water removed. In industrial settings, this must be balanced against batch throughput when designing trays and process parameters.

5. Conclusion

A three-dimensional conjugate heat and mass transfer model, calibrated with pilot-scale data, was developed for the vacuum freeze-drying of mare milk using COMSOL's *Deformed Geometry* interface. Simulated centre-line temperature profiles tracked experimental measurements closely achieving R^2 = 0.96. The model also located the sublimation front to within 4 % of image-analysis observations, confirming its capability to describe primary-drying behaviour with engineering accuracy.

Simulation-experiment comparisons showed that (i) decreasing chamber pressure from 35 Pa to an optimised 15 Pa shortens primary-drying time by 2.6 h and cuts specific energy consumption by 22 %; further pressure reduction yields marginal benefit (≤ 4 %), (ii) reducing product thickness from 7 mm to 3 mm halves the diffusion path and decreases drying time by roughly 40 %, and (iii) temperature and vapour gradients remain one-dimensional in the slab centre, validating common scale-up assumptions.

The COMSOL model developed in this work serves as a physics-based tool for choosing chamber-pressure set-points and tray thicknesses that balance energy demand with throughput while preserving the nutritional and sensory quality of mare-milk powder.

Future work will focus on (a) integrating real-time sensor data for closed-loop pressure control, (b) coupling the model with nutrient-degradation kinetics to predict quality retention, and (c) collaborating with industrial partners to validate the framework in commercial freeze-dryers operating at square-metre scale.

Data Availability

The raw temperature–time and moisture-loss datasets (CSV format) that support the findings of this study are openly available at https://github.com/Arshynbek/Freeze-drying- accessed 31 May 2025). The accompanying COMSOL. mph model (≈100 MB) exceeds common repository size limits and will therefore be provided by the corresponding author, on reasonable request, via a secure file-transfer link.

Acknowledgements

This research was funded by the Committee of Science, the Ministry of Science and Higher Education of the Republic of Kazakhstan (grant no. BR21881957).

Conflict of Interest

There is no conflict of interest.

Supporting Information

Applicable.

CRediT statement

Arshyn Altybay: Original draft, Writing – review & editing, Methodology, Resources, Investigation. **Symbat Satybaldy**: Writing – review & editing, Software, Formal analysis, Methodology, Data curation. **Ayaulym Rakhmatulina**: Investigation, Formal analysis, Supervision, Resources, Project administration, Funding acquisition.

References

[1] A. Musaev, S. Sadykova, A. Anambayeva, M. Saizhanova, G. Balkanay, M. Kolbaev, Mare's milk: composition, properties, and application in medicine, *Archives of Razi Institute*, 2021, **76**, 1125-1135, doi: 10.22092/ari.2021.355834.1725.

[2] A. Kushugulova, S. Kozhakhmetov, R. Sattybayeva, A. Nurgozhina, A. Ziyat, H. Yadav, F. Marotta, Mare's milk as a prospective functional product, *Functional Foods in Health and Disease*, 2018, **8**, 548, doi: 10.31989/ffhd.v8i11.528.

[3] C. Ratti, Hot air and freeze-drying of high-value foods: a review, *Journal of Food Engineering*, 2001, **49**, 311-319, doi: 10.1016/S0260-8774(00)00228-4.

[4] M. J. Pikal, Freeze Drying, *Encyclopedia of Pharmaceutical Technology*, Taylor and Francis, London, 2006, 1180-1291, 084939399X, 9780849393990

[5] T. Kramer, D. M. Kremer, M. J. Pikal, W. J. Petre, E. Y. Shalaev, L. A. Gatlin, A procedure to optimize scale-up for the primary drying phase of lyophilization, *Journal of Pharmaceutical Sciences*, 2009, **98**, 307-318, doi: 10.1002/jps.21430.

[6] J. F. Nastaj, K. Witkiewicz, Mathematical modeling of the primary and secondary vacuum freeze drying of random solids at microwave heating, *International Journal of Heat and Mass*

Transfer, 2009, **52**, 4796-4806, doi: 10.1016/j.ijheatmasstransfer.2009.06.015.

[7] J. F. Nastaj, K. Witkiewicz, B. Wilczyńska, Experimental and simulation studies of primary vacuum freeze-drying process of random solids at microwave heating, *International Communications in Heat and Mass Transfer*, 2008, **35**, 430-438, doi: 10.1016/j.icheatmasstransfer.2007.09.003.

[8] A. I. Liapis, R. J. Litchfield, Optimal control of a freeze dryer: I theoretical development and quasi steady state analysis, *Chemical Engineering Science*, 1979, **34**, 975-981, doi: 10.1016/0009-2509(79)85009-5.

[9] K. Georgiev, N. Kosturski, S. Margenov, J. Starý, On adaptive time stepping for large-scale parabolic problems: Computer simulation of heat and mass transfer in vacuum freeze-drying, *Journal of Computational and Applied Mathematics*, 2009, **226**, 268-274, doi: 10.1016/j.cam.2008.08.020.

[10] M. M. Tang, A. I. Liapis, J. M. Marchello, A multi-dimensional model describing the lyophilisation of a pharmaceutical product in a vial, *Advances in Drying*, Hemisphere Publishing Corporation, London, 1986, 57-64.

[11] M. J. Millman, A. I. Liapis, J. M. Marchello, An analysis of the lyophilization process using a sorption-sublimation model and various operational policies, *AIChE Journal*, 1985, **31**, 1594-1604, doi: 10.1002/aic.690311003.

[12] B. Scutellà, S. Passot, E. Bourlés, F. Fonseca, I. C. Tréléa, How vial geometry variability influences heat transfer and product temperature during freeze-drying, *Journal of Pharmaceutical Sciences*, 2017, **106**, 770-778, doi: 10.1016/j.xphs.2016.11.007.

[13] C. J. King, Freeze-drying of foods, CRC Press, Cleveland, 1971, 1-54, ISBN: 9780878191055.

[14] R. J. Litchfield, A. I. Liapis, An adsorption-sublimation model for a freeze dryer, *Chemical Engineering Science*, 1979, **34**, 1085-1090, doi: 10.1016/0009-2509(79)85013-7.

[15] A. I. Liapsis, J. M. Marchello, Advances in the modelling and control of freeze drying, *Advances in Drying*, Hemisphere Publishing Corporation, Washington, 1984, 217–244, 978-089116297-1.

[16] W. J. Mascarenhas, H. U. Akay, M. J. Pikal, A computational model for finite element analysis of the freeze-drying process, *Computer Methods in Applied Mechanics and Engineering*, 1997, **148**, 105-124, doi: 10.1016/S0045-7825(96)00078-3.

[17] B. Scutellà, A. Plana-Fattori, S. Passot, E. Bourlès, F. Fonseca, D. Flick, I. C. Tréléa, 3D mathematical modelling to understand atypical heat transfer observed in vial freeze-drying, *Applied Thermal Engineering*, 2017, **126**, 226-236, doi: 10.1016/j.applthermaleng.2017.07.096.

[18] G. Srinivasan, M. Muneeshwaran, B. Raja, Numerical investigation of heat and mass transfer behavior of freeze drying of milk in vial, *Heat and Mass Transfer*, 2019, **55**, 2073-2081, doi: 10.1007/s00231-018-02538-1.

[19] W. M. El-Maghlany, A. E. Bedir, M. Elhelw, A. Attia, Freeze-drying modeling *via* multi-phase porous media transport model, *International Journal of Thermal Sciences*, 2019, **135**, 509-522, doi: 10.1016/j.ijthermalsci.2018.10.001.

[20] B.-L. Chen, J.-H. Jang, M. Amani, W.-M. Yan, Numerical and experimental study on the heat and mass transfer of kiwifruit during vacuum freeze-drying process, *Alexandria Engineering Journal*, 2023, **73**, 427-442, doi: 10.1016/j.aej.2023.05.025.

[21] Z. Khamitkyzy, A. Kistaubayeva, I. Savitskaya, D. Shokatayeva, S. Zhantlessova, Optimized food-grade semi-synthetic culture medium and freeze-drying approach with antidiabetic cryoprotectants for akkermansia muciniphila, *ES Food & Agroforestry*, 2025, **21**, 1634, doi: 10.30919/faf1634.

[22] Z. Zhu, H. Zhang, Y. Ma, Z. Yang, Z. Chen, H. Zhang, Preparing high-quality monolithic carbon nanotubes reinforced silica aerogel composites based on a vacuum freeze-drying method, *Engineered Science*, 2024, **31**, 1149, doi: 10.30919/es1149.

[23] A. Rakhmatulina, A. Altybay, N. Imanbayeva, S. Bagitova, A. Baikonys, Numerical simulation and experimental analysis of mare's milk sublimation drying, *Processes*, 2025, **13**, 206, doi: 10.3390/pr13010206.

[24] A. Altybay, A. Rakhmatulina, D. Darkenbayev, S. Satybaldy, Energy-efficient vacuum sublimation drying of camel milk: numerical simulation and parametric analysis, *Energies*, 2025, **18**, 3665, doi: 10.3390/en18143665.

[25] E. Lopez-Quiroga, L. T. Antelo, A. A. Alonso, Time-scale modeling and optimal control of freeze–drying, *Journal of Food Engineering*, 2012, **111**, 655-666, doi: 10.1016/j.jfoodeng.2012.03.001.

[26] M. Malacarne, F. Martuzzi, A. Summer, P. Mariani, Protein and fat composition of mare's milk: some nutritional remarks with reference to human and cow's milk, *International Dairy Journal*, 2002, **12**, 869-877, doi: 10.1016/S0958-6946(02)00120-6.

[27] C. S. Song, J. H. Nam, C. J. Kim, S. T. Ro, Temperature distribution in a vial during freeze-drying of skim milk, *Journal of Food Engineering*, 2005, **67**, 467-475, doi: 10.1016/j.jfoodeng.2004.04.041.

[28] J. H. Nam, C. S. Song, Numerical simulation of conjugate heat and mass transfer during multi-dimensional freeze drying of slab-shaped food products, *International Journal of Heat and Mass Transfer*, 2007, **50**, 4891-4900, doi: 10.1016/j.ijheatmasstransfer.2007.08.004.

[29] A. Altybay, N. Tokmagambetov, Numerical simulation and parallel computing of acoustic wave equation in isotropic heterogeneous media, *Computer Modeling in Engineering &*

Sciences, 2024, **141**, 1867-1881, doi: 0.32604/cmes.2024.054892